Thermo-catalytic depolymerization of lignin over Pd-based catalysts: Role of catalyst support on monoaromatics selectivity

José R. Colina[1,2], Maray Ortega[1], Jose Norambuena-Contreras[3], Stef Ghysels[4], Frederik Ronsse[4], Luis E. Arteaga-Pérez[5*]

[1]Laboratory of Thermal and Catalytic Processes (LPTC), Wood Engineering Department, University of Bío-Bío, Concepción, 4030000, Chile.

[2]Facultad de Medicina y Ciencia, Universidad San Sebastián, Lientur 1457, Concepción 4080871, Chile

[3]Materials and Manufacturing Research Institute, Department of Civil Engineering, Faculty of Science and Engineering, Swansea University, Bay Campus, SA1 8EN, UK.

[4]Department of Green Chemistry and Technology, Ghent University, Coupure Links 653, Ghent 9000, Belgium

[5]Department of Chemical Engineering, Faculty of Engineering, Universidad de Concepcion, Chile

*Corresponding author: luiseap@gmail.com

Graphical Abstract

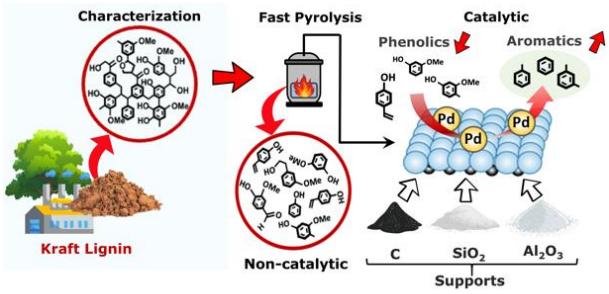

Abstract

The condensed structure of technical lignin presents significant challenges in converting it into valuable functionalized building blocks, such as single-ring aromatics. In this study, we explored how palladium-based catalysts influence the selectivity of monoaromatics during the fast pyrolysis depolymerization of lignin. A systematic study on the influence of the pyrolysis temperature ($500 < T < 700$ ºC) and catalyst support nature (SiO_2, Al_2O_3 and Carbon) was carried out by analytical pyrolysis. Creosol and guaiacol were the predominant species after non-catalytic and Pd/SiO_2 catalyzed pyrolysis of Kraft lignin. However, when Pd/C and Pd/Al_2O_3 were applied, the selectivity to monoaromatics increased drastically, to 50.9% and 34.4%, respectively. The catalytic activity of Pd/C and Pd/Al_2O_3 was ascribed to the presence of medium and weak acid sites in the supports, which provides active sites for phenolics adsorption and deoxygenation. Additionally, metallic Pd sites activated the C-O and H_2 bonds to further assist deoxygenation reactions, thus inducing a bifunctionality to these materials. This study offers valuable insights into the bifunctional effects of supported catalyst during the thermo-catalytic depolymerization of lignin.

Keywords: Depolymerization; Fast pyrolysis; Kraft lignin; monoaromatics; Catalysts.

1. Introduction

The fast development of the world's population has increased the demand for fuels and chemicals, posing substantial environmental, social, and economic issues. In recent years, significant efforts have focused on creating technologies and methods that use non-edible biomass to produce valuable chemical compounds, aligning with the United Nations' Sustainable Development Goals [1].

In such circumstances, lignin, one of the three principal components of lignocellulosic biomass, has received a lot of interest for its potential as a platform for creating chemical building blocks [2]. The global production of technical lignin is approximately 100 million metric tons per year, making it one of the most readily available feedstocks for the synthesis of biofuels and biochemicals [3].

Nonetheless, only around 2% of technical lignin is commercially used for low-value goods, with the rest used as low-grade fuel in heat and power plants, often to power pulp mills [4,5].

Technical lignin is generated as a byproduct during the delignification process of lignocellulosic biomass in paper manufacturing facilities. The structure and properties of technical lignin are influenced by the biomass source and extraction methods employed. Consequently, various types of technical lignin can be produced based on the delignification process utilized, including Kraft, Lignosulfonate, Organosolv, and Soda, among others [6].

Kraft lignin represents the predominant form of lignin extracted in the paper industry, comprising approximately 85% of the total lignin extraction process. The Kraft process entails the depolymerization of lignin in alkaline conditions, utilizing Na_2S and NaOH. This process generally requires heating the material for a duration of up to 1 hour at temperatures ranging from 170 to 180 °C. The process leads to the production of a solution referred to as black liquor, from which kraft lignin is extracted following its precipitation through acidification [7].

Lignin is a phenolic biopolymer composed of phenyl propane units, specifically guaiacyl alcohol (G), syringyl alcohol (S), and 4-hydroxyphenyl alcohol (H), in a complicated 3D structure [8]. Given its aromatic structure, lignin is a desirable feedstock for the manufacture of chemicals and fuels with a variety of applications. However, because of the high degree of condensation in technical lignin, its value is severely limited. Various conversion strategies have been investigated for converting raw technical lignin into useful chemicals and fuels. Among other approaches, depolymerization of lignin via oxidation, hydrotreating, solvolysis, and pyrolysis has received a lot of interest.

Pyrolysis has proven to be an effective approach for breaking down lignin's complicated 3D structure into smaller subunits. In fast pyrolysis, lignin is rapidly heated at temperatures between 450 - 800 ºC in the absence of oxygen, producing bio-oil, char, and light gasses [9–11]. The composition of bio-oil varies depending on the type of lignin used and the treatment conditions, but it often contains high levels of phenolics (with selectivity ranging from 60 to 80%) as well as other organic oxygenated compounds such aldehydes, ketones, and carboxylic acids [12,13]. However, fast pyrolysis of lignin

has low selectivity for aromatics. In fact, the bio-oils generated are multicomponent mixtures with limited thermal and chemical stability [9,14]. The specialized generation of customized chemicals can be done by selecting appropriate catalysts [15,16].

Catalytic fast pyrolysis is an excellent method for improving the quality and stability of bio-oils [17]. Typically, the catalytic upgrading of lignin bio-oils necessitates the activation of C-O groups and H_2 on the catalyst surface [10]. As a result, this process is often carried out at high temperatures and high hydrogen pressures, converting phenol-rich bio-oils into alicyclic and aromatic hydrocarbons [18]. The majority of investigations in this field have concentrated on the utilization of zeolite systems such as H-ZSM-5, H-MCM-41, H-beta, mordenite, ferrierite, and H-USY, as well as metal salts and metal oxides [9,15]. Nonetheless, zeolite-based systems are susceptible to deactivation due to carbon deposition during the catalytic cracking of pyrolysis gasses. Furthermore, the presence of water deactivates the catalyst by dealumination or by tailoring the nature of acid sites. As a result, some authors have recommended using metal-supported catalysts to improve deoxygenation, focusing on noble-metal catalysts (such as Pd, Pt, Rh, and Ru) that are distinguished by their ability to activate and dissociate H_2 on their surfaces [19]. In addition to the features of the metal site, the kind of support has a considerable impact on the activity and selectivity of the catalysts. The surface properties of the support, in particular, specific area, acid density, nature of acid sites, can tailor the catalyst's performance by creating new active sites in the vicinities of the metal via strong metal-support interactions (SMSI), generating new Lewis' sites with hydrogen spill-over capacity, and so on [20,21]. Teles et al., [59] investigated the efficacy of Pd-based catalysts for HDO of lignin model compounds (phenol, m-cresol, anisole, and guaiacol) in the vapor phase at 573 K. The authors demonstrated that the activity and selectivity for deoxygenated products are substantially correlated with the support characteristics regardless of the model molecule. Thus, benzene and toluene were the leading products of the Nb-supported catalysts, whereas cyclohexanone and methylcyclohexanone were the primary molecules produced on Pd/SiO_2. It has also been established that HDO can create benzene and toluene from bio-oil-related platform molecules (benzaldehyde, benzyl alcohol, phenyl acetate, and anisole)

via catalysts including Pt and Pd supported on Al_2O_3 [22]. More recently, Kim et al. [23] employed Ru, Pd, and Ru-Re supported in activated carbon to deoxygenate Kraft lignin pyrolysis byproducts, yielding a hydrocarbon combination suitable for gasoline, jet fuel, and diesel fuels. In that work, activated carbon outperformed strong acidic supports like H-ZSM-5 and TiO_2 at deoxygenating lignin derivatives. These findings were attributable to the poor adsorption of phenolic compounds onto the carbon support. While the foregoing data show catalytic efficacy, difficulties remain, such as catalyst deactivation, coke production, and catalysts' reduced capacity to convert the broad variety of chemicals created by lignin depolymerization into aromatic hydrocarbons. Furthermore, there is a need to design a stable catalyst capable of selectively removing oxygenated groups from lignin pyrolysis products while using little or no hydrogen.

Thus, here we study how various supports impact the performance of Pd-based catalysts in converting Kraft lignin pyrolysis byproducts into valuable monoaromatic hydrocarbons without the presence of hydrogen. The catalytic performance of palladium nanoparticles for lignin depolymerization at various temperatures was investigated by supporting them on SiO_2, Al_2O_3, and activated carbon. The selection of SiO_2, Al_2O_3, and activated carbon as supports was based on their distinct acid nature, metal-support interactions, and industrial significance. While existing literature has documented studies on the catalytic conversion of phenolics or lignin model compounds to aromatics, systematic reports on the influence of catalyst supports on the selective production of monoaromatics from lignin pyrolysis are scarce.

This study presents the first exploration of the effects of Pd supported on SiO_2, Al_2O_3, and activated carbon on Kraft lignin pyrolysis in the absence of an external hydrogen source. It aims to shed light on the role of support materials in enhancing the efficiency of noble metal-based catalysts for converting lignin derivatives into monoaromatics. The findings offer a potential pathway toward developing sustainable methods for producing aromatic hydrocarbons from renewable resources.

2. Materials and methods

2.1 Lignin characterization

Stora Enso (Helsinki, Finland) kraft lignin was subjected to elemental and proximate analysis using a Leco CHNS 628 elemental analyzer and a muffle furnace in accordance with ASTM D5373-21 [24] and ASTM D3172-13 [25] standards. A Netzsch STA 409PC thermal analyzer was used to perform thermal gravimetric analysis (TGA). The TGA was performed from room temperature to 800 ºC using a N_2 atmosphere (50 mL min^{-1}) and a heating rate of 10 ºC min^{-1}. Moreover, lignin Fourier transformed infrared spectroscopy (FTIR) spectra were acquired using a Nicolet is20 (Thermo Fisher, USA) spectrometer fitted with an attenuated total reflection accessory (Specac Golden Gate ATR, UK) with a Ge crystal. The investigation covered the Mid-IR spectral range of 4000-600 cm^{-1}, with spectra averaged from 32 scans at a resolution of 4 cm^{-1}.

2.2. Catalysts preparation

Pd-based catalysts supported on SiO_2, Al_2O_3 and activated carbon were used to infer the role of the support properties (bulk acidity, acid site´s nature and textural properties) on the catalytic conversion of pyrolysis vapors. The Pd/C was obtained from Merck (CAS-87104, Merck Group) in the form of an oxide (10% Pd). Pd/SiO_2 and Pd/Al_2O_3, were prepared by incipient wetness impregnation onto SiO_2 (Sigma-Aldrich, CAS-112926-00-8) and Al_2O_3, (Sigma-Aldrich, CAS-1344-28-1). Incipient wetness impregnation was carried out with suitable volumes of a $PdCl_2$ solution (59% Pd, Sigma-Aldrich, CAS-7647-10-1) at a pH of about 1.5. Triethanolamine (TEA, ≥99.0%, Merck Group, CAS-102-71-6) was utilized to create a uniform distribution of the metal on the supports, following the procedure outlined by Soled et al. [26]. Next, the catalysts underwent a calcination process for 4 hours at 500 ºC to eliminate any remaining TEA and create oxidized precursors. The precursors were reduced in a U-shaped quartz reactor with a 6 mm inner diameter under a flow of H_2 at a rate of 40 mL min^{-1}. The reduction process took place in an electrically controlled tube furnace at a temperature of 400 °C, with a heating rate of 2 °C min^{-1} and a dwell time of 2 hours. A schematic representation of the experimental setup for catalyst reduction is shown in Fig. 1.

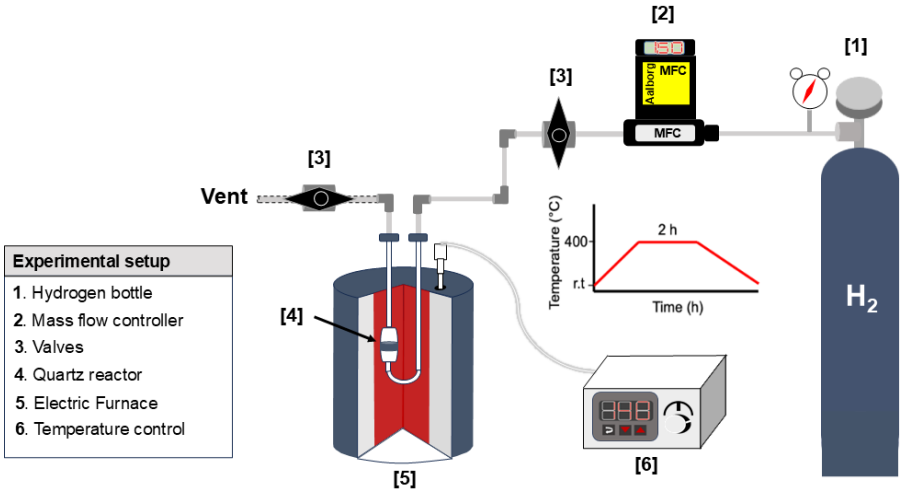

Figure 1. Experimental setup for the catalyst reduction process.

2.3. Catalysts characterization

Experiments were conducted at 77 K to investigate the textural properties of catalysts by nitrogen adsorption on Pd/SiO_2, Pd/Al_2O_3, and Pd/C. The specific surface areas and pore volumes were determined using the Brunauer–Emmett–Teller (BET) model and Barrett–Joyner–Halenda (BJH) method, respectively. The isotherms were recorded using a 3Flex instrument (Micromeritics, USA). The catalyst samples underwent a 24-hour outgassing process at 150 ºC under vacuum conditions. The reducibility of the Pd-based catalysts was investigated by temperature-programmed reduction (TPR) assays. The experiments were conducted from ambient temperature to 600ºC and H_2 signal was followed by a thermal conductivity detector (TCD) in an ASAP 2010 apparatus (Micromeritics, USA). Moreover, bulk acidity of catalysts was quantified by ammonia thermal programmed desorption (TPD-NH_3) in a 3Flex device (Micromeritics, USA) interfaced with a mass spectrometer (Cirrus 2, MKS Instruments) [27].

An infrared spectroscopic analysis of the adsorption and desorption of pyridine (C_5H_5N, J.T. Baker, >99.9%) was conducted to examine the nature of surface acid sites (Lewis or Brønsted). The experiment was performed with catalysts discs (13 mm, 10 mg) placed in an IR flow cell, which had

ZnSe windows and a vacuum system (Pfeiffer Hicube Eco Turbo). The samples underwent outgassing at a pressure of 0.1 mPa and a temperature of 450 °C, with a heating rate of 5 °C min^{-1}, for a duration of 10 hours. Next, the spectrum of the clean samples was obtained as a baseline, and the process of pyridine adsorption was started at a temperature of 150 °C for a duration of 30 minutes. Afterwards, the process of desorption was conducted at temperatures of 25, 140, 250, and 400 °C for a duration of 30 minutes each. The IR spectra for each desorption temperature were obtained using a Nicolet iS50 (ThermoScientific, USA) instrument equipped with an MCT detector. The spectra were taken at a resolution of 4 cm^{-1}, using 32 scans.

The effective metal content of the catalysts was determined using atomic absorption spectrometry (AAS) on a Perkin Elmer 3100 apparatus (Perkin Elmer, Manasquan, NJ, USA). Prior to the analysis, the samples were microwave-digested with 50 mg of catalyst and 10 mL of concentrated HNO_3/HCl. The catalysts were morphologically characterized using transmission electron microscopy (TEM) with a JEOL JEM 1200 EXII microscope at 120 kV. The TEM images were analyzed using the software ImageJ to estimate the particle size distribution using the volume-weighted function proposed by Vannice (eq. (1)) [28]:

$$d_{pi} = \frac{\sum_{j=1}^{n} n_j \times d_{pj}^4}{\sum_{j=1}^{n} n_j \times d_{pj}^3} \quad \text{(Eq. 1)}$$

Further, the metal dispersion supposing a hemispherical particle shape was calculated using Eq. (2).

$$D = \frac{6 \times \left(\frac{V_m}{a_m}\right)}{d_p} \quad \text{(Eq. 2)}$$

Where D represent the Pd dispersion, V_m is the volume occupied by an atom in the bulk metal (14.7 $Å^3$), a_m is the area occupied by a surface atom (7.93 $Å^2$), and d_p is the average particle size obtained from TEM images.

High resolution images and electron diffraction patterns of the catalysts also were acquired by high-resolution transmission electron microscopy (HRTEM) using a JEOL JEM-2200FS (JEOL, Japan) microscope with double aberration correction operated at 200 kV.

X-ray diffraction (XRD) patters of Pd-based catalysts were acquired using a Bruker D4 Endeavour diffractometer with Cu Kα radiation (λ = 0.154 nm) operating at 40 kV and 20 mA. The XRD data were collected in the range of 2θ = 3–90º at a speed of 0.02º s^{-1}. The crystalline structure of the catalysts was determined by a search–match procedure using the Mercury 3.7 software and the Crystallography Open Database. The particle sizes were calculated by means of the Scherrer equation (Eq. (3)) [29,30]:

$$L = \frac{K \times \lambda}{\beta \times \cos(\theta)} \quad \text{(Eq. 3)}$$

In this equation, *L* is the crystallite size in nm, *K* is the crystallite shape factor whose numerical value of 0.90 is accepted [30], β is the full width at half maximum (in radians) of the main peak and θ is the Bragg´s angle of diffraction peak measured in radians.

2.4. Lignin catalytic pyrolysis

The lignin catalytic pyrolysis experiments were conducted using a micropyrolysis system (Py-GC-MS) that included a CDS 5200 Pyroprobe HPR micropyrolyzer (CDS analytical, USA), a Clarus 690 gas chromatograph (Perkin Elmer, USA), and a Clarus SQ-8T MS detector mass spectrometer (Perkin Elmer, USA). For the experiment, a quartz tube was used to hold the sample, which consisted of 500 µg of Kraft lignin. The tube was packed with quartz wool to ensure the sample remained in place. Then, catalysts were positioned on either side of the sample to direct the pyrolysis vapors through the catalyst bed. The pyrolysis assays were conducted at temperatures of 500, 600, and 700 ºC in an inert He atmosphere. The temperature range was selected based on previous literature reports for the same lignin [31–34]. The heating rate was set at 10 °C ms^{-1} until the pyrolysis temperature was reached, and this was maintained for a time of 6 s. During the experiment, the pyrolysis products are flushed out of the reaction zone by a carrier gas (pure He, 99.999% purity from Airliquide-Chile) and trapped in a Tenax trap until GC analysis. For catalytic experiments, the lignin-to-catalysts mass ratio was set at 1:5, inspired by previous investigations [35–37]. A detailed illustration of the experimental setup and methodology is presented in Fig. 2. Preliminary pyrolysis experiments were conducted at 700 ºC

to verify the intrinsic activity of the catalyst supports (SiO_2, Al_2O_3, and C). For these experiments SiO_2 (CAS-112926-00-8) and Al_2O_3 (CAS- 1344-28-1) were from Sigma-Aldrich and activated carbon (CAS- 7440-44-0) was purchased from PhytoTech Labs. The GC oven was set to maintain a temperature of 45 ºC for 1 minute, followed by a gradual increase to 260 ºC at a rate of 4 ºC per minute. Helium was utilized as a carrier gas with a flow rate of 50 mL/min. In all the experiments, the pyrolysis interface and the GC injector were kept at a constant temperature of 280 °C. The products obtained from pyrolysis were separated using a Perkin Elmer Elite 1701 capillary column, measuring 30 m × 2.5 µm. Compound identification consisted of contrasting the mass spectra (m/z range of 40-500 Da) with the National institute of standards and technology (NIST) mass spectral library v2.2 and crosschecking with relevant literature. Experiments were conducted in triplicate to ensure consistency, and the reported data represents the average of the three tests. Prior to conducting the experiments, the lignin was subjected to a drying process at 105 °C for 12 hours. The peak area (i)/mass of the sample was used as a representation of the quantity of the products from pyrolysis.

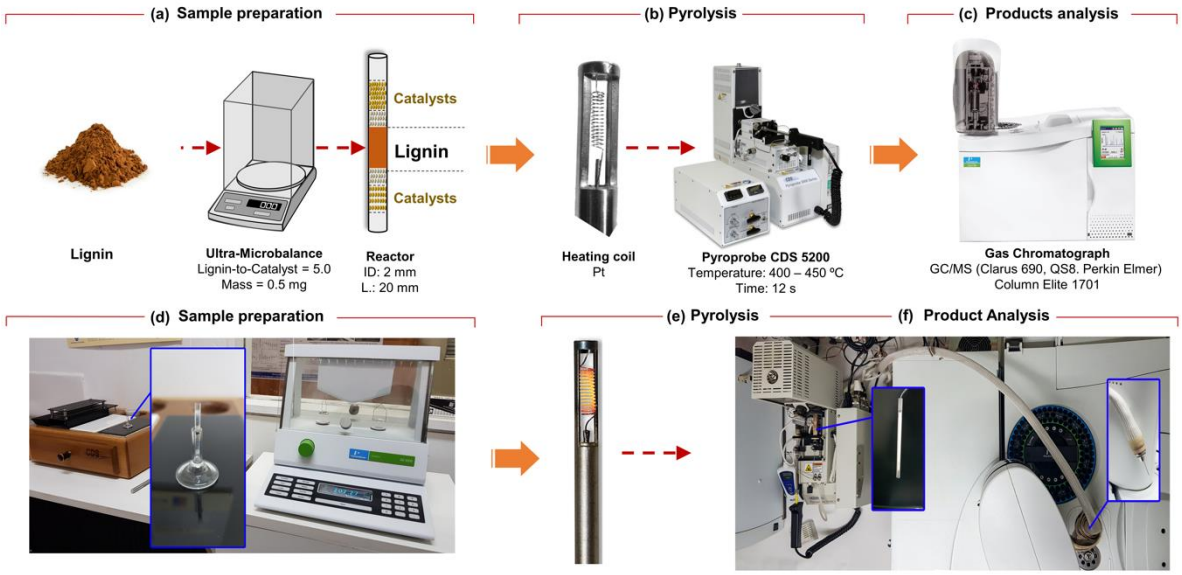

Figure 2. Experimental setups and sequential steps for lignin catalytic pyrolysis experiments. Modified from Smith et al. [38] with permission of Elsevier.

3. Results and discussion

3.1. Lignin characterization

The results from the proximate and elemental analysis of Kraft lignin are presented in Table 1. Kraft lignin exhibits a significant amount of volatile matter and an extremely low ash content. However, a considerable amount of moisture was detected in the samples during the analysis, even though a pre-drying step was not performed. According to reports, pyrolysis processes are not suitable for moisture content exceeding 30% [39,40]. Thus, the lignin samples underwent a 12-hour drying process at 105 ºC to eliminate any moisture before conducting the chemical characterization and Py-GC-MS experiments. The elemental analysis results align with the findings of other Kraft lignin documented in the literature [41–43], confirming the high relative C content and the presence of S-species. It is worth noting that sulfur is not naturally found in lignin. However, during Kraft pulping, sulfur is introduced into the lignin structure in the form of aliphatic thiol, sulfide, and disulfide groups [4,43,44]. Finally, the nitrogen detected (0.15 %) could potentially be attributed to protein-lignin associations [45].

FTIR spectra of Kraft lignin (Fig. 3) reveal a prominent and wide absorption band at 3500 cm^{-1}, resulting from the stretching vibration of O-H groups in phenolic and aliphatic hydroxyl groups, along with residual water content in the sample. Confirmation of the presence of aliphatic chains attached to aromatic rings was obtained from the absorption peak observed at 2938 cm^{-1}. This signal is associated with the symmetrical stretching vibration of C-H in aliphatic side chains [46]. The absorption band at 1708 cm^{-1} is attributed to the stretching vibration of non-conjugated carbonyl groups, while the peaks observed at 1600 and 1516 cm^{-1} are a result of the stretching vibration of the benzene ring skeleton and phenolic hydroxyl C−OH, respectively. An absorption band at 1460 cm^{-1} indicates the deformation of C-H stretching, while a small peak at 1360 cm^{-1} suggests the presence of phenolic hydroxyl groups.

Table 1. Results from proximate and elemental analysis of Kraft lignin.

Proximate composition	**(wt. %)**	**Elemental composition**	**(wt. %)**
Moisture	34.90 ± 0.29	C	65.37 ± 0.15
Fixed carbon*	30.56 ± 0.16	H	5.63 ± 0.22
Volatile matter*	68.87 ± 0.44	O+	26.63 ± 0.18
Ash*	0.57 ± 0.02	N	0.14 ± 0.01
		S	1.65± 0.02

* Estimated from dry lignin; +O was obtained by difference of C, H, N, S and Ash on dried lignin samples.

In addition, there are vibrations at 1266 cm^{-1}, 1144 cm^{-1}, 860 cm^{-1}, and 817 cm^{-1} that correspond to specific guaiacyl units. These vibrations indicate C-O stretching, C-H in-plane deformation, and C-H out-of-plane vibrations at positions 2, 5, and 6 of the guaiacyl ring, respectively [47,48]. There is an absorption band at 1215 cm^{-1} that is related to stretching of C-C and C-O bonds, and another peak at 1035 cm^{-1} that corresponds to deformation of aromatic C-H bonds. Based on the FTIR results, it can be inferred that Kraft lignin primarily comprises guaiacyl units.

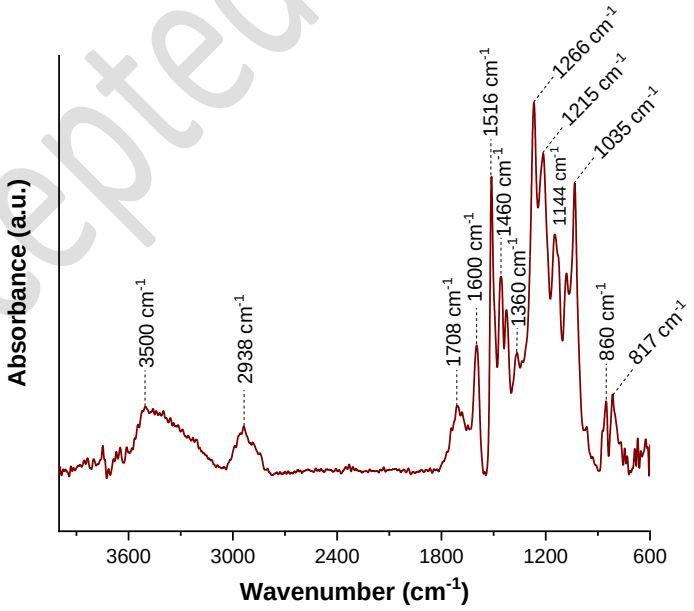

Figure 3. FTIR spectra of Kraft lignin showing the position of major IR signals ascribed to phenolic, aromatic and aliphatic functional groups.

The TG/DTG curves of Kraft lignin (Fig. 4) exhibit three significant thermal events (stages) from room temperature to 800 ºC. In stage I, there was a slight weight loss (2%) which was due to the removal of moisture that was physically bound in lignin [49]. Following that, a secondary and significant phase took place within the temperature range of 150-500 ºC. This phase was marked by a distinct peak on the derivative of the thermogravimetric curve (DTG), which was centered around 400 ºC. This peak, associated to devolatilization and depolymerization of the backbone structure in lignin results in a 45% weight loss. It involves the breaking of aryl-ether bonds such as β-O-4 and α-O-4, as well as the separation of short-chain substituents from the aromatic rings. Given the width of stage II, it is believed that within this temperature range, various volatile components of different structures and mass distributions may be released. These components can be seen as potential candidates for catalytic upgrading [1,44]. In the third stage (500–800 ºC), the breakdown of carbon-carbon bonds in the lignin structure occurs, which are more resistant to thermal degradation. It is possible that the 10% weight loss observed in this stage is due to the formation of larger molecules and the bonding of carbon structures in the remaining chars, resulting in the release of CO and CO_2 [50]. After the experiment concluded, a solid mixture of biochar and ash accounted for approximately 43% of the original weight of the sample.

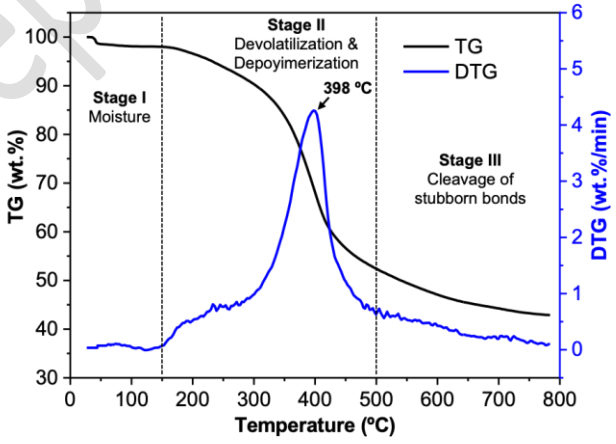

Figure 4. TGA/DTG curves of Kraft lignin. Lignin sample was dried at 105 ºC for 24 h prior to the assay.

The thermal properties and composition of lignin indicate that thermal depolymerization has the potential to be a useful method for generating phenolics and monoaromatics from lignin. For optimal devolatilization of lignin, it is recommended to use a pyrolysis temperature range above 500 ºC. Nevertheless, upgrading of pyrolysis products continues to be a difficult endeavor. One possible solution to this challenge is to use catalysts that have certain chemical and physical properties.

3.2. Characterization of catalysts for lignin depolymerization

Figures 5a to 5f display the N_2 adsorption-desorption isotherms and pore size distributions of Pd/SiO_2, Pd/Al_2O_3, and Pd/C, respectively. The isotherms for Pd/SiO_2 (Fig. 5a) and Pd/Al_2O_3 (Fig. 5b) exhibit a type-IV classification as per the IUPAC. In addition, the hysteresis loops closing at p/p_0= 0.4 indicate an H1 type hysteresis, which is commonly observed in mesoporous materials. The results are consistent with the pore size distributions, which exhibit narrow bimodal curves centered at 16, 10.5 and 2.8 nm (Fig. 5d-5f). This confirms that the catalysts used are indeed mesoporous materials [51]. Meanwhile, Pd/C exhibited a hysteresis loop of type H3 (p/p_0 = 0.4), which is commonly associated with capillary condensation in plate-like pores. The isotherm shape confirms the existence of some micropores, a characteristic often observed in activated carbons [52].

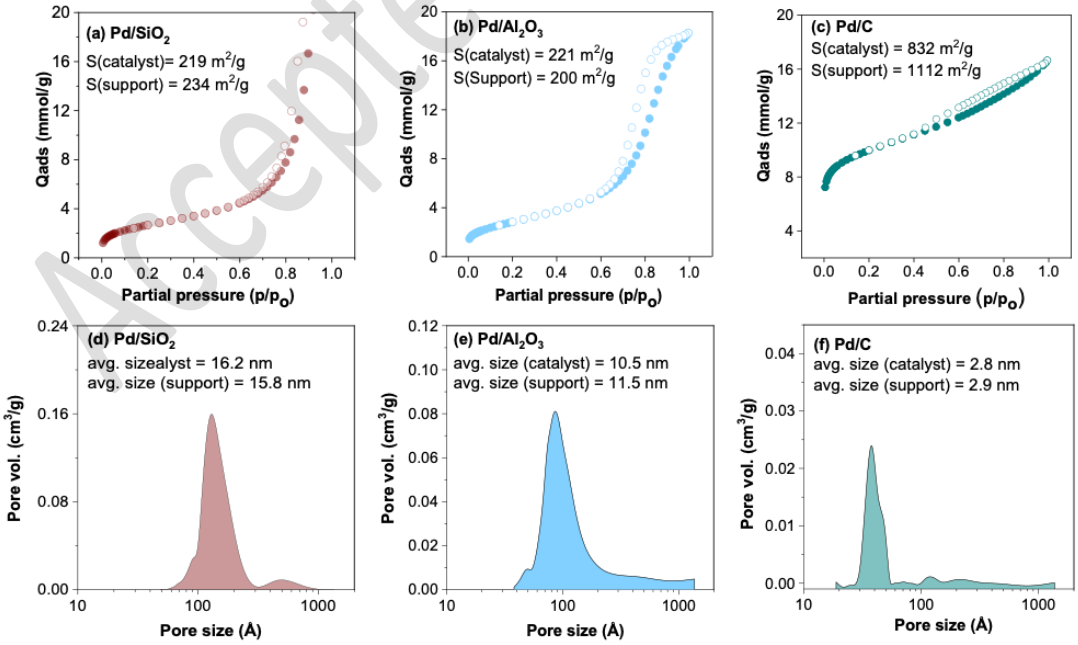

Figure 5. N_2-physisorption isotherms of a) Pd/SiO_2; b) Pd/Al_2O_3 and c) Pd/C.

In addition, the surface area calculated using BET's model for the Pd/SiO_2 and Pd/Al_2O_3 catalysts were found to be similar (Table 2). However, the Pd/C catalyst exhibited a higher surface area, which aligns with previous findings for activated carbons [53,54]. The surface areas and average pore sizes of the catalysts align with those measured for the supports, indicating an effective dispersion of the metallic nanoparticles during synthesis. The minor increase in the Pd/SiO_2 area compared to that of the support can be attributed to the heat treatments applied, specifically calcination and reduction, which may induce a pore opening effect. The surface of the carbon support underwent partial reduction after the impregnation of Pd nanoparticles, likely due to its narrower pore size compared to other supports. This suggests that the majority of the particles are effectively dispersed across the surface of the support.

Table 2. Physical properties of the Pd-based catalysts on three different supports.

Catalyst	**Surface area ($m^2\ g^{-1}$)**	**Metal content (%wt.)**	**Particle size (nm)[a]**	**Particle size (nm)[b]**	**Dispersion (%)**
Pd/SiO_2	219	9.35 ±0.08	8.6	4.6 ± 1.0	24
Pd/Al_2O_3	221	8.95 ±0.6	6.6	3.6 ± 0.7	30
Pd/C	832	9.37 ±0.6	5.8	3.3 ± 1.1	33
SiO_2	234	n.a.	n.a.	n.a.	n.a.
Al_2O_3	200	n.a.	n.a.	n.a.	n.a.
Carbon	1112	n.a.	n.a.	n.a.	n.a.

[a] Determined using Scherrer equation (eqn. 1); [b] Determined from TEM micrographs using eq. 2.

The Pd content in the catalysts confirmed the effectivity of the synthesis method, and the similarity in metallic composition for Pd/SiO_2, Pd/C and Pd/Al_2O_3. The values of metal content in Table 2 were used to determine the lignin-to-catalyst ratio during the pyrolysis experiments.

Given the high surface area and the well-dispersed Pd nanoparticles on the catalyst surface, effective catalytic performance for the upgrading of pyrolysis vapors can be achieved. The elevated surface area of catalysts facilitates active sites for species adsorption, whereas the dispersion of Pd

nanoparticles may enhance reactions involving highly coordinated Pd atoms, such as hydrogenation of C=O and C=C. Furthermore, the presence of mesopores enhances the diffusion of molecules into the catalyst pores, reducing mass transport limitations during catalytic experiments.

The TPR profiles in Figure 6a exhibit intense peaks at low temperatures (<150 ºC). There are sharp peaks observed at 76 ºC for Pd/SiO_2 and Pd/C, which could be due to the reduction of surface PdO or the conversion of PdO to Pd-β hydrides [55–57]. On the other hand, the wide peaks observed between 85 – 130 ºC indicate the conversion of Pd^{2+} to Pd^0 [58,59]. Based on the TPR analysis results, it is possible to achieve a significant amount of zero-valence Pd on the catalyst surface by reducing Pd/SiO_2, Pd/Al_2O_3, and Pd/C under the same conditions.

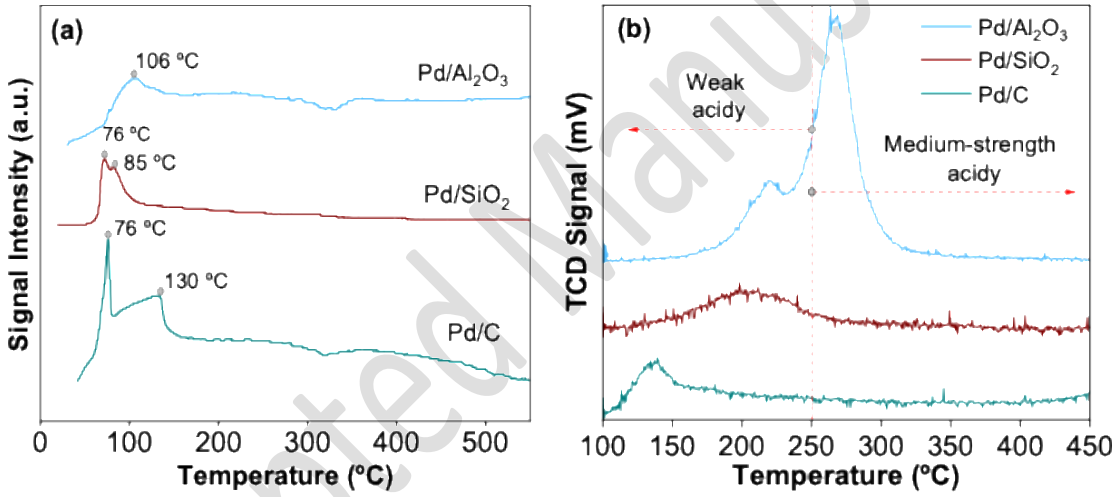

Figure 6. a) Temperature programmed reduction profiles and b) Temperature programmed desorption of NH_3 profiles of the Pd-based catalysts.

Fig. 6b displays the assessment of the acidic properties of Pd/SiO_2, Pd/Al_2O_3, and Pd/C catalysts using Temperature-Programmed Desorption (TPD) of NH_3. Acidic site strength was determined by analyzing the temperature at which the NH_3 desorption peaks occurred. Typically, desorption peaks below 250 °C indicated the presence of weak acid sites, while NH_3 desorption peaks above 450 °C were observed for strong acid sites. Peaks observed in the temperature range of 250 to 450 ºC were attributed to medium acid sites [27,60]. Desorption peaks below 250 ºC were observed in the TPD

analysis for all catalysts, suggesting the existence of weak acidic sites. The Pd/SiO_2 displayed a low density of acid sites, which is commonly observed in SiO_2 supports. On the other hand, Pd/Al_2O_3 exhibited a strong peak at 280 ºC, suggesting the presence of mainly medium acid sites in this material. Finally, the Pd/C showed a wide peak between 120 – 150 ºC, possibly indicating the existence of weak acid sites.

Based on the TPD-NH_3 results, it is evident that the three catalysts have different characteristics and levels of acidity. These variations could potentially impact the conversion of pyrolytic lignin derivatives into monoaromatics by providing active sites for adsorption, hydrogen spillover from metallic sites and via intrinsic activity for cracking, dealkylation and other acid-promoted reactions.

The nature of catalysts' surface acidic sites was examined using pyridine adsorption/desorption and FTIR spectroscopy. The Pd/SiO_2 catalyst exhibits two primary peaks at 1446 and 1596 cm^{-1}, indicating coordinated pyridine at Lewis acid sites. The Pd/Al_2O_3 catalyst showed peaks at 1493, 1578, 1615, and 1623 cm^{-1}, also indicating pyridine coordination at Lewis sites. The Lewis sites found in Pd/Al_2O_3 correspond to exposed Al^{3+} sites and are characterized as medium (1578-1596 cm^{-1}) or high strength acidity (1615-1623 cm^{-1}) [61,62]. The FTIR-PyR for these catalysts showed no signals at 1545 cm^{-1}, indicating that none of the catalysts have Brønsted acid sites. Finally, the quantification of the Lewis acidity Pd/SiO_2 and Pd/Al_2O_3 catalysts, was performed at 140 °C using Emeis' molar extinction coefficient for the peak at 1446 cm^{-1} (2.22 cm μmol^{-1}) [63], while that of Pd/C was determined by Wu et al [64]. The results confirms that the concentration of Lewis acid sites was ordered as Pd/Al_2O_3 (371 $\mu mol\ g_{cat}^{-1}$) > Pd/C (151 $\mu mol\ g_{cat}^{-1}$) > Pd/SiO_2 (95 $\mu mol\ g_{cat}^{-1}$).

TEM images and particle size distribution (PSD) histograms are shown in Figures 7a to 7g for Pd/SiO_2, Pd/Al_2O_3, and Pd/C catalysts. The TEM images show clear outlines of Pd nanoparticles evenly distributed on the supports. The dispersion values for Pd in these materials were arranged in the following order: 24% for Pd/SiO_2, 30% for Pd/Al_2O_3, and 33% for Pd/C. Having a higher dispersion and smaller particle size can lead to a more robust metal-support interaction, which may improve the stability and activity of the catalysts when they are used in reactions to produce

monoaromatics [65]. Furthermore, the consistent dispersion patterns among these materials indicate that any significant variations in product distribution can be attributed to their acid character rather than any structural or textural factors.

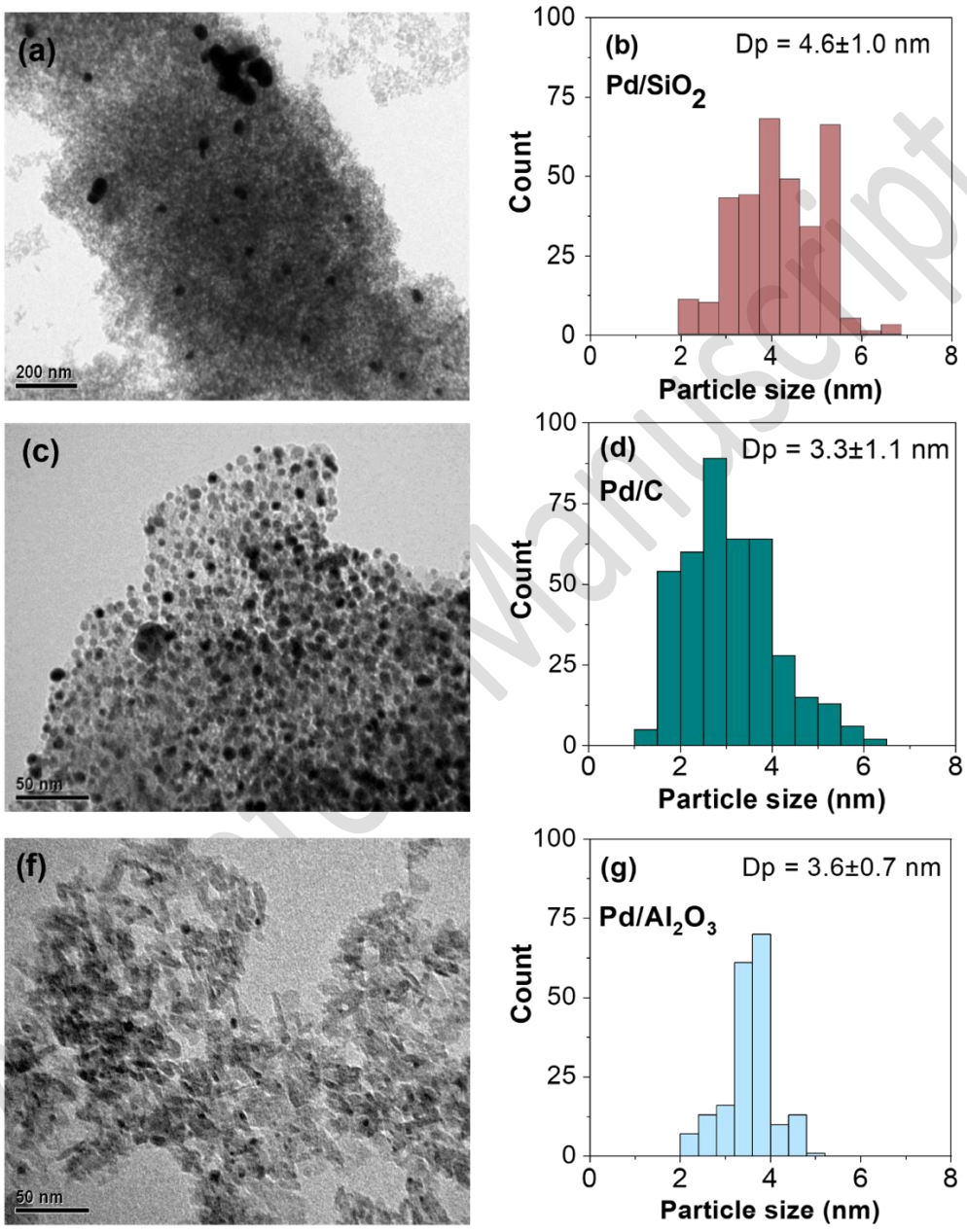

Figure 7. TEM images and particle size distribution for: a-b) Pd/SiO_2; c-d) Pd/Al_2O_3 and f-g) Pd/C.

After reduction, the X-ray diffraction (XRD) patterns of the catalysts (refer to Fig. 8) show the presence of identical diffraction peaks at specific angles. These angles correspond to the planes of

metallic Pd with a face-centered cubic (f.c.c) structure. The peaks are observed at 2θ = 40.1°, 46.7°, 68.1°, 82.1°, and 86.7°, representing the (111), (200), (220), (311), and (222) planes, respectively. The existence of these planes was also verified through e-diffraction from HRTEM (inserts in Fig. 8). Just by looking at the HRTEM images, one can easily spot distinct variations in the surface facets of the Pd nanoparticles. These differences can have a profound effect on the catalysts' performance, especially in reactions that are sensitive to the structure. For example, the sharp peaks seen in Pd/SiO_2 suggest slightly larger Pd particles, than those found for Pd/Al_2O_3 and Pd/C. The diffractograms of Pd/Al_2O_3 and Pd/C show broader peaks, which can be explained by the smaller particle size and better dispersion of Pd on these supports, which aligns with the findings from TEM analysis. In addition, it was noticed that the average particle sizes obtained through XRD using the Scherrer equation (refer to Table 2) were considerably larger compared to those determined from TEM micrographs. These variations may be due to the increased diffraction broadening caused by imperfections in the crystal lattice [27]. While there may be some deviations in the values of particle size obtained from TEM, they are generally considered to be more accurate than those estimated from XRD [66].

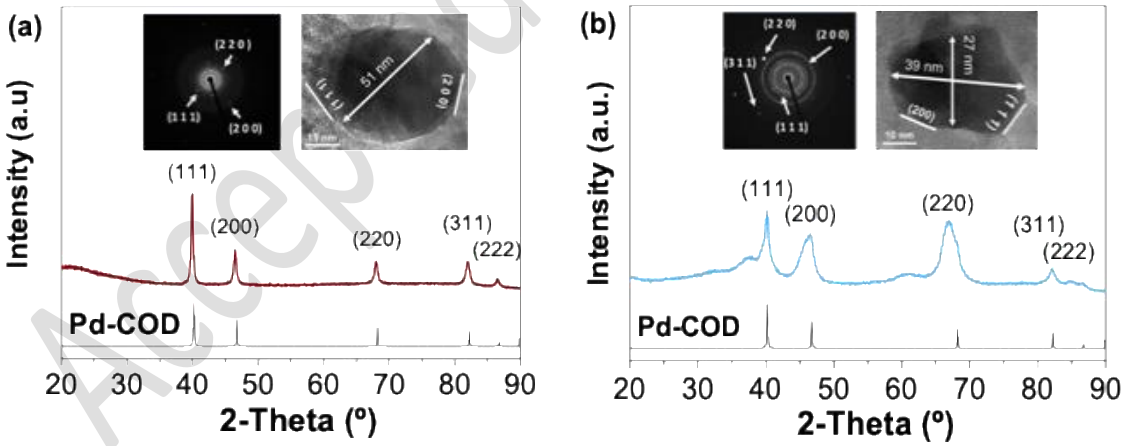

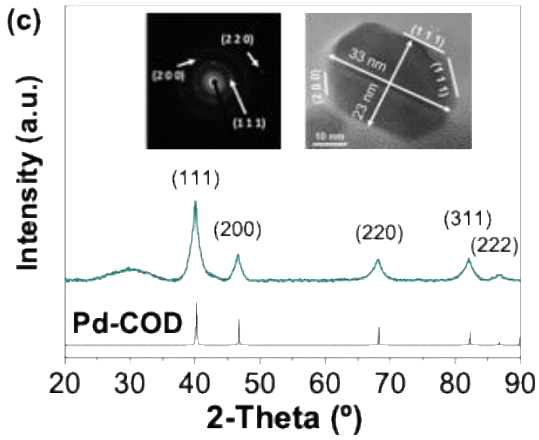

Figure 8. X-ray diffraction patters of a) Pd/SiO_2; b) Pd/Al_2O_3 and c) Pd/C. Standards from the COD database are inserted in the figures for Pd^0 (1011105) (http://www.crystallography.net/cod/).

3.3. Product distribution from catalytic and non-catalytic pyrolysis of Kraft lignin

For this study, we thoroughly investigated how the Pd-support and reaction temperature affect the products from Kraft lignin fast pyrolysis in an inert atmosphere. Figure 9 illustrates the distribution of primary products based on their chemical groups resulting from non-catalytic and catalytic pyrolysis of Kraft lignin at temperatures of 500, 600, and 700 ºC. In Fig. 9a, the results of non-catalytic pyrolysis show that lignin depolymerization took place within the temperature range studied, producing mainly substituted phenols (83–90%). The lignin-derived phenols are produced when ether linkages, such as β-O-4 and α-O-4, in the lignin backbone are broken down [67]. In addition, non-catalytic pyrolysis produced a small amount of monoaromatic hydrocarbons (2 – 7%), such as benzene and toluene. These aromatics can be formed through various chemical reactions, such as demethoxylation, dealkylation, or via reductive cleavage reactions. These mostly endothermic reactions are favored by increase of the temperature as confirmed here by the yield's trends (green bars in Figure 7a) [14,68]. Our analysis also detected the presence of oxygenates (non-phenols) and sulfur- and nitrogen-containing compounds (8 – 10%), which are classified as "others". The initial observations from lignin pyrolysis confirm the necessity of applying catalytic processes to achieve a fine tuning of product selectively towards aromatics.

During the experiment with Pd/SiO_2 (Fig. 9b), there were no significant changes in the selectivity of chemical groups compared to non-catalytic pyrolysis. Although metal-SiO_2 catalysts have shown efficacy in the hydrodeoxygenation (HDO) of lignin model compounds, at elevated H_2 pressures [68–70]; our results indicate that the activity of Pd/SiO_2 for upgrading pyrolysis vapors is constrained under H_2 depleted conditions. This is because several organic molecules, such as alkyl phenols, can adsorb onto SiO_2 at the same time. This increases the catalytic surface coverage, thereby reducing the reaction rate for relevant kinetic steps. This phenomenon may also occur on Al_2O_3 and carbon, but these supports have shown intrinsic activity in promoting C-C bond-breaking, -OH activation, and dealkylations over acid sites (Fig. S2), which could explain their enhanced performance. On the other hand, despite Pd^0 sites facilitating the dissociation of H_2 generated in situ during pyrolysis, the existence of Lewis acid sites in Al_2O_3 and carbon supports adjacent to Pd^0 would increase the activity for hydrogenation reactions through H_2 spillover, a phenomenon not observed with mild acid supports like SiO_2 [12, 14, 69].

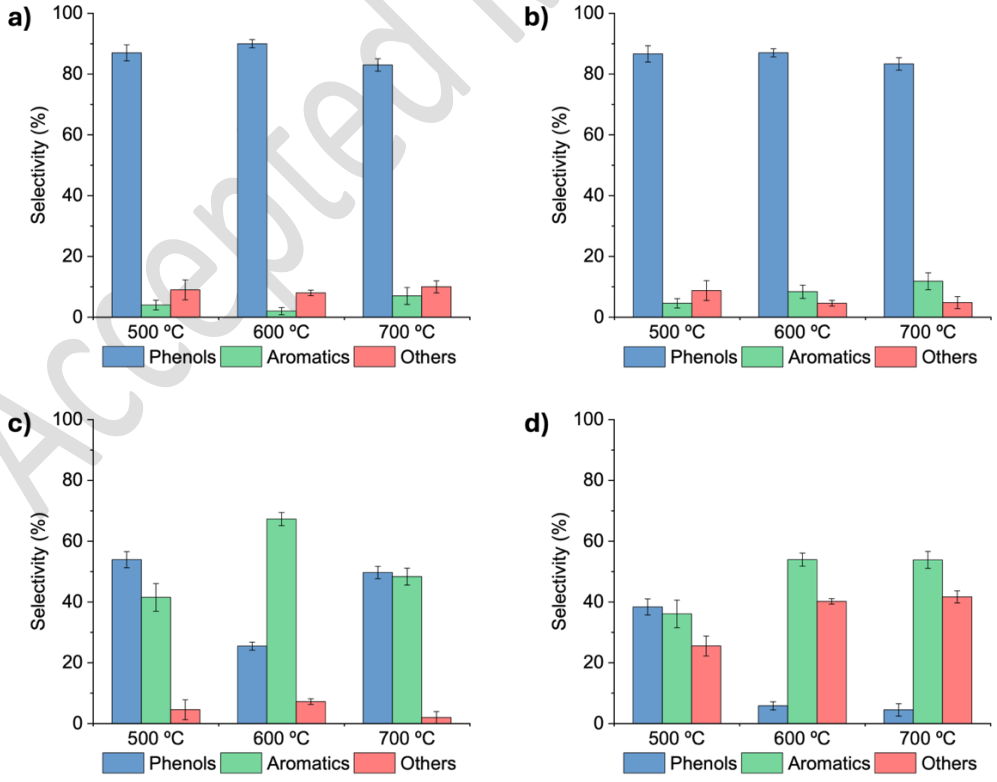

Figure 9. Distribution of the main chemical groups identified in the product of non-catalytic and catalytic lignin pyrolysis. a) non-catalyst, b) Pd/SiO_2, c) Pd/C and d) Pd/Al_2O_3.

The compositional trends for Pd/C and Pd/Al_2O_3, presented noticeable differences in the distribution of primary chemical groups (Fig.7c and 7d). The selectivity towards monoaromatics varied with temperature, reaching peak values of 67% and 42% at 600 ºC for Pd/C and Pd/Al_2O_3, respectively. These observations indicate that variations in the support´s nature and concentration of acid sites have a significant impact on the conversion of primary products from lignin pyrolysis. Remarkably, the acidity of catalysts reduced the phenol abundance in pyrolysis products in the following decreasing order: non-catalytic>Pd/SiO_2>Pd/C>Pd/Al_2O_3. This trend demonstrates a connection between catalyst supports and product distribution from lignin pyrolysis, but it does not confirm bifunctionality or a direct correlation with the nature of acid sites. Thus, in the upcoming section, we will investigate in depth how the nature of the catalyst's support acid sites affects the product distribution from Kraft lignin catalytic pyrolysis.

3.4. Role of catalyst support in Kraft lignin thermo-catalytic depolymerization

Building upon the first examination outlined in Section 3.3, we investigate the role of support in Pd-based catalysts in enhancing the production of monoaromatics from the catalytic fast pyrolysis of lignin. Since phenolics are important in this system because they are the building blocks for aromatics, we focused our research on these groups to find out how the acid sites in the catalyst support contributes to their production.

Catalytic fast pyrolysis experiments were conducted using pristine SiO_2, Al_2O_3, and activated carbon, at 1:5 support-to-lignin ratios. The results demonstrated that activated carbon and Al_2O_3 possess inherent catalytic activity on the products from depolymerization of lignin (Fig. S2). The product distribution from support-catalyzed pyrolysis demonstrates that acid sites in the support contributes to dealkylation and C-C bond scission in phenolics. However, the monoaromatic yield from these assays was not different from that obtained under non-catalytic conditions, indicating that Pd sites are

required to promote the conversion of phenolics into aromatics. The inherent activity of supports indicates that their combination with metal sites, will results in a bifunctional activity promoting aromatic formation from lignin pyrolysis.

According to our previous observations, catalytic pyrolysis assays were conducted on Pd/SiO_2, Pd/Al_2O_3, and Pd/C at three different temperatures to identify the main products obtained from lignin depolymerization (Fig. 10a – 10d).

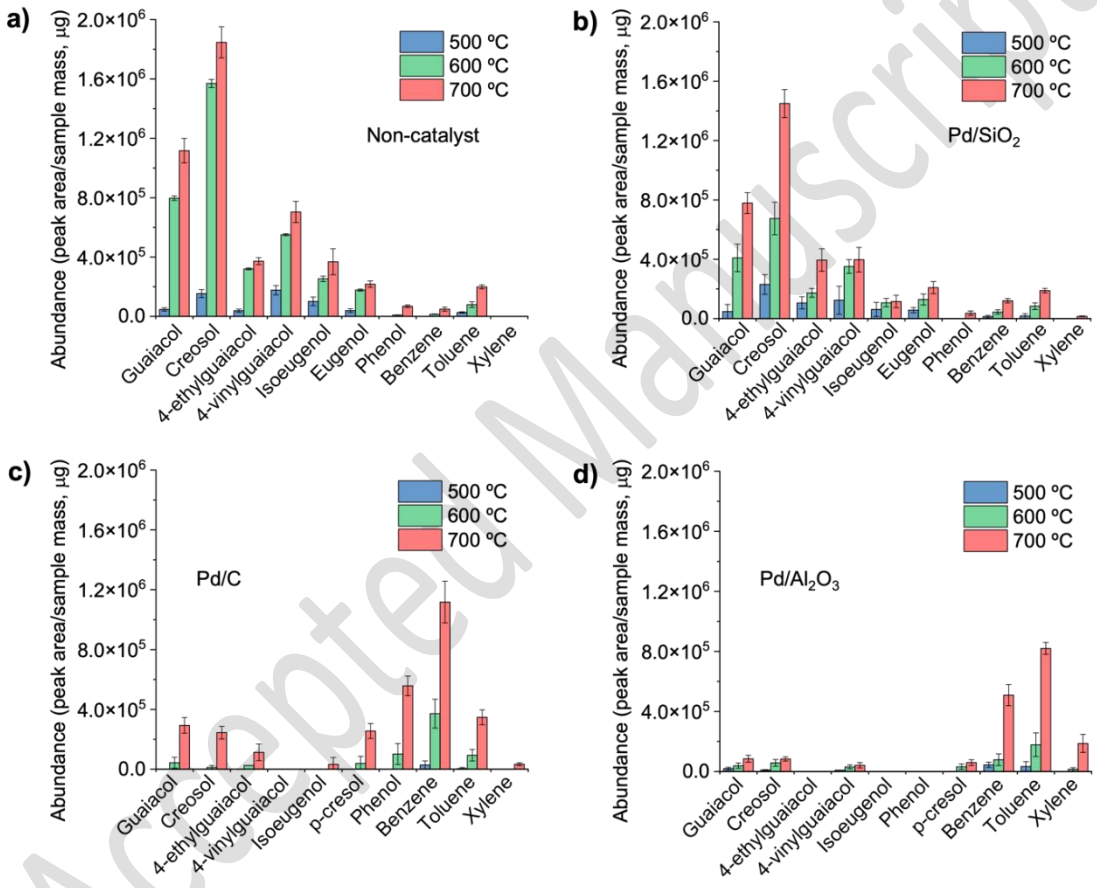

Figure 10. Relative quantities of majority products obtained from non-catalytic and catalytic lignin pyrolysis at different temperatures.

The main compounds identified from non-catalytic pyrolysis (Fig. 10a) were methoxylated phenols such as creosol, guaiacol, and 4-vinylguaiacol. Further, a higher abundance of phenolic compounds can be observed with increasing pyrolysis temperature, which align with the observations of Figueiredo et al. and Fan et al. [12,14].

Conversely, significant differences in product distribution from catalytic pyrolysis were observed depending on the nature of the support and the temperature.

The product distribution from Pd/SiO_2 catalyzed pyrolysis was similar to that from non-catalytic pyrolysis, indicating that Pd nanoparticles on inert supports exhibit limited catalytic activity. Lu et al. [69] reported high catalytic activity of Pd/SiO_2 for the hydrogenation of guaiacol. However this showed limited deoxygenation activity, which was mainly attributed to the low acidity of the support. Indeed, deoxygenation activity could be enhanced by employing high H_2 pressures, inducing bifunctionality through support acid-base properties, or promoting a strong metal support interaction (SMSI).

The previous hypothesis on the bifunctionality or metal-acid supports for enhancing lignin pyrolysis is confirmed by inspecting the product distribution for Pd/C and Pd/Al_2O_3 (Fig. 10c and 10d). These figures show a remarkable shift in the distribution from substituted phenolics to monoaromatics *viz.* benzene, toluene and xylene. Apparently, the yield of monoaromatics increased at expense of phenolics, indicating that deoxygenation reactions are effectively catalyzed over Pd/C and Pd/Al_2O_3. Figure 8c reveals the presence of phenol and p-cresol in the products of Pd/C catalysis, which is consistent with previous reports [70]. These compounds may originate from the elimination of the methoxy moiety of guaiacol and creosol, which exhibited a significant decrease in relative abundance compared to non-catalytic experiments. Sun et al. [70], demonstrated that Pd/C exhibits significant activity for demethoxylation and hydrodeoxygenation of guaiacol, which resulted in significant yields of phenol, and oxygen-free aromatic compounds during vapor-phase catalytic reactions.

In Figure 8d, the abundance of benzene, toluene, and xylene in the presence of Pd/Al_2O_3 is evident, although their relative quantity was lower than that achieved with Pd/C. Additionally, low abundance of phenols is observed, indicating that Pd/Al_2O_3 exhibits high catalytic activity for phenols conversion but lower selectivity to monoaromatics than Pd/C. The outstanding activity of Pd/Al_2O_3 to convert oxygenated compounds has also been demonstrated by Majhi et al. [71]. In this study, the oxygen

content of bio-oils obtained from deodar and pine was reduced from 43.64% and 41.58% to 1.98% and 1.54%, respectively.

For Pd/C and Pd/Al_2O_3 catalyst, the abundance of aromatics (e.g., BTX) at 500 ºC, was barely noticeable. This result is interesting, as we previously confirmed (Fig. 9c and 9d) the selectivity to aromatics at the same operational conditions was above 40%. This apparent contradiction can be explained by a low rate of lignin depolymerization and aromatization at this temperature, which could lead to low yields of pyro-oils while selectivity keeps high [70].

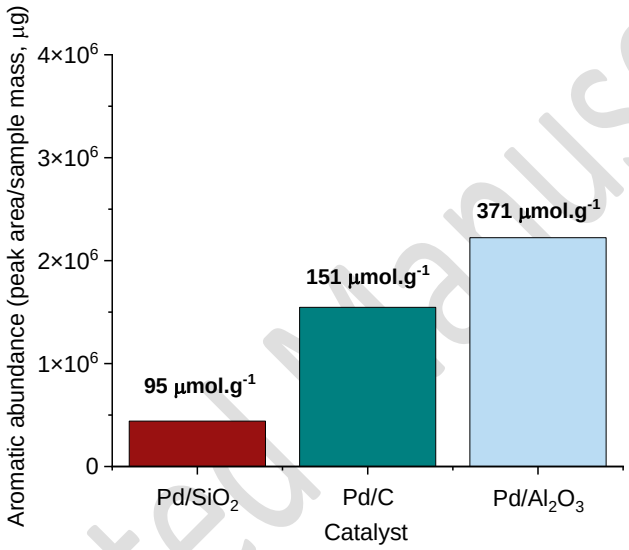

Figure 11. Aromatics abundance from catalytic lignin Kraft pyrolysis at 700 °C and Lewis acid sites concentration of Pd-based catalysts.

From Fig. 11, a correlation between aromatics abundance and Lewis's acid sites concentration in the Pd-based catalysts can be observed, demonstrating the prominent role played by the density of acid sites in selectivity to monoaromatics. The presence of Lewis acid sites on the supports, particularly in Pd/C and Pd/Al_2O_3, provide active sites for phenolics adsorption and their conversion to monoaromatics via deoxygenation. In Pd/Al_2O_3, the high concentration of Lewis acid sites, in addition to deoxygenation, could promote side reactions such as dealkylation, alkylation and decarbonylation leading to a greater variety of products (Fig. 10d). Furthermore, the acid character

of the support could offer sites for cracking reactions, resulting in a high yield of light gases and olefins (not shown here).

The observed catalytic conversion of phenols into monoaromatics over acid catalysts, aligns with recent findings by Zhang et al. [72], who reported the conversion of phenol and phenol derivatives from catalytic fast pyrolysis of Kraft lignin to benzene, toluene, and xylene using NbOP and NbO as catalysts. The authors proposed that direct deoxygenation of lignin take place by both sp^2 and sp^3 C–O cleavage. Moreover, they explain this effect -even in the absence of an external H_2 source- to catalyst properties such as strong acidity, ample surface area -especially on the external surface- and uniform mesopore sizes.

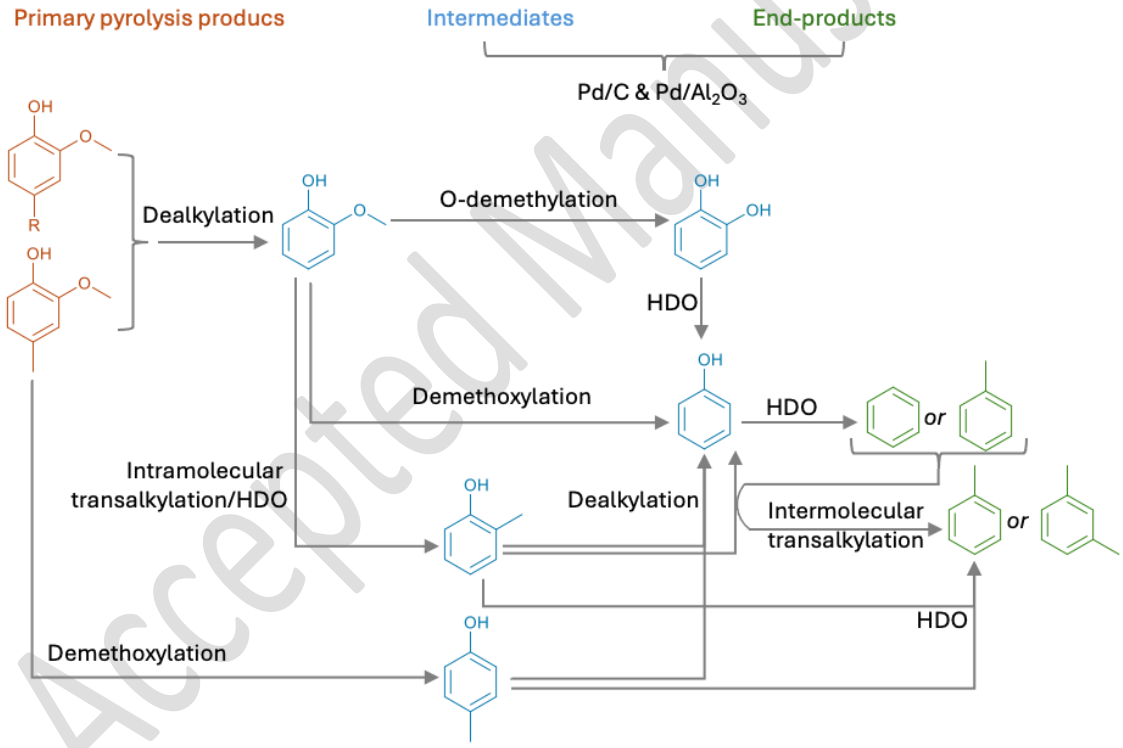

Figure 12. Putative reaction map, showing the conversion of primary Kraft lignin pyrolysis products into its observed intermediates and end-products, using no or the mentioned Pd-based catalysts.

Finally, our results demonstrated that Pd/C and Pd/Al_2O_3 can promote deoxygenation reactions in a H_2-depleted atmosphere via deoxygenation reactions. Moreover, the product distribution also

suggests that deoxygenation of phenolics and their conversion into aromatics can also take place via consecutive trans hydrogenation and deoxygenation, both occurring by a bifunctional effect of the Pd (111) facets and support acid sites. According to these observations, the reaction scheme shown in Fig.12 was drawn:

The chemical reaction map shown in Fig. 12, is constructed based on the abundance and anticipated relation between the observed pyrolysis compounds from Fig. 10 and the nature of catalyst support. During the pyrolysis of Kraft lignin without the use of a catalyst, a significant presence of alkylated (methoxy) phenols was detected (Fig. 12, orange). Among these, creosol, a type of methoxylated phenol, was found to be the most abundant. This is consistent with other micropyrolysis studies [70]. By using Pd/Al_2O_3 and Pd/C, several intermediate compounds (shown in blue in Figure 12) are hypothesized to be formed, ultimately resulting in the products observed in Figure 10. Cresol, particularly p-cresol, and phenol have been identified as key chemical intermediates in the production of benzene, toluene, and xylene through catalytic vapor-phase upgrading using Pd/C and Pd/Al_2O_3. However, notable differences in the proportion of these products were obtained from each catalyst. Phenol and p-cresol were among the major products from the Pd/C catalysis, while they were scarcely detected when Pd/Al_2O_3 was used. In addition, appreciable abundance of styrene and ethylbenzene was also found in the products (data not shown) from lignin catalyzed pyrolysis over Pd/Al_2O_3, which can be ascribed to demethoxylation and subsequent hydrogenation of 4-vinylguaiacol, respectively. This shows that the higher concentration of Lewis acid sites facilitates the occurrence of a greater variety of reactions on the Pd/Al_2O_3 catalyst. It is worth noting that cresol can be formed through intramolecular transmethylation and dehydration of guaiacol [73]. Additionally, cresol can be obtained by demethoxylation of creosol [74]. Continued dehydration of cresol results in the formation of toluene (Fig. 10c and 10d). Phenol is a significant intermediate that can be derived from guaiacol. It remains abundant when catalyzed with Pd/C (Fig 10c). However, when using a more acidic support (Pd/Al_2O_3), catalytic pyrolysis results in a decrease in phenolics and an increase in toluene. There may be two possible explanations for this; (i) phenol undergoes a hydrodeoxygenation process to

produce benzene, which is then further transformed into toluene and xylenes through intermolecular transalkylations or (ii) p-cresol could be transformed by HDO into toluene.

4. Conclusions

In this study, we investigated the effect of different type of supports (SiO_2, Al_2O_3, C) in Pd-based catalyst for the selective production of monoaromatics via catalytic fast pyrolysis of Kraft lignin in absence of external hydrogen. From non-catalytic and Pd/SiO_2 catalyzed experiments, mainly methoxy phenols (creosol, guaiacol and 4-vinylguaiacol) were obtained, while on Pd/C and Pd/Al_2O_3 the lignin pyrolysis products were successfully converted into monoaromatic hydrocarbons (benzene, toluene, and xylene), reaching yields of 50.9 % and 34.4 %, respectively. Utilizing the transalkylation of phenol, demethoxylation of creosol, and hydrogenation of other OH- containing species are promoted on Pd/C and Pd/Al_2O_3 catalysts due to the synergistic effect between the metal sites and the support. Additionally, the pyrolysis temperature plays a significant role in the catalytic cycle, because it affects the interaction between the initial breakdown of lignin and the subsequent catalytic upgrading of vapors. Although Pd sites controls hydrogenation processes by activating H_2, when Pd is supported on non-acidic materials like SiO_2, it does not show significant activity in enhancing monoaromatic selectivity. This finding indicates that the presence of a bifunctional Metal-Support system is crucial for modulating the selectivity of the products. The results obtained demonstrated that Pd/C and Pd/Al_2O_3 are promising catalysts for bio-oil upgrading for the production the valuable chemicals and biofuel.

Declaration of competing interests

The authors declare that they have no known competing financial interests or personal relationships that could have appeared to influence the work reported in this paper.

CRediT authorship contribution statement

José R. Colina: Writing – original draft, Investigation, Formal analysis, Data curation and project administration. **Maray Ortega:** Investigation – Formal analysis, Data curation **Luis E. Arteaga-Pérez:** Writing – review & editing, Methodology, Conceptualization. **Jose Norambuena-Contreras:**

Writing – review & editing, Supervision. **Stef Ghysels–** data analysis, writing original draft, review & editing. **Frederik Ronsse:** Writing original draft, Resources, Methodology, Conceptualization.

Acknowledgments

The authors thank the financial support given by the National Research and Development Agency (ANID) through the Research Projects FONDECYT Postdoctoral Grant 3230605, FONDECYT Regular Grant 1240054 and FONDEQUIP 170077 as well as to Johnson Matthey for providing $PdCl_2$ through the PGM award program.

5. References

[1] H. Wang, Y. Pu, A. Ragauskas, B. Yang, From lignin to valuable products–strategies, challenges, and prospects, Bioresour Technol 271 (2019) 449–461. https://doi.org/10.1016/J.BIORTECH.2018.09.072.

[2] F. Brienza, D. Cannella, D. Montesdeoca, I. Cybulska, D.P. Debecker, A guide to lignin valorization in biorefineries: traditional, recent, and forthcoming approaches to convert raw lignocellulose into valuable materials and chemicals, RSC Sustainability 2 (2024) 37–90. https://doi.org/10.1039/D3SU00140G.

[3] G. Iakovou, D. Ipsakis, K.S. Triantafyllidis, Kraft lignin fast (catalytic) pyrolysis for the production of high value-added chemicals (HVACs): A techno-economic screening of valorization pathways, Environ Res 248 (2024) 118205. https://doi.org/10.1016/J.ENVRES.2024.118205.

[4] O. Gordobil, R. Moriana, L. Zhang, J. Labidi, O. Sevastyanova, Assesment of technical lignins for uses in biofuels and biomaterials: Structure-related properties, proximate analysis and chemical modification, Ind Crops Prod 83 (2016) 155–165. https://doi.org/10.1016/J.INDCROP.2015.12.048.

[5] M. Alekhina, O. Ershova, A. Ebert, S. Heikkinen, H. Sixta, Softwood kraft lignin for value-added applications: Fractionation and structural characterization, Ind Crops Prod 66 (2015) 220–228. https://doi.org/10.1016/J.INDCROP.2014.12.021.

[6] A. Ekielski, P.K. Mishra, Lignin for Bioeconomy: The Present and Future Role of Technical Lignin, International Journal of Molecular Sciences 2021, Vol. 22, Page 63 22 (2020) 63. https://doi.org/10.3390/IJMS22010063.

[7] B.F.M.L. Gomes, S. Vaz Júnior, L.V.A. Gurgel, Production of activated carbons from technical lignin as a promising pathway towards carbon emission neutrality for second-generation (2G) ethanol plants, J Clean Prod 450 (2024) 141648. https://doi.org/10.1016/J.JCLEPRO.2024.141648.

[8] H. Guo, Y. Zhao, J.S. Chang, D.J. Lee, Lignin to value-added products: Research updates and prospects, Bioresour Technol 384 (2023) 129294. https://doi.org/10.1016/J.BIORTECH.2023.129294.

[9] X. Lu, X. Gu, A review on lignin pyrolysis: pyrolytic behavior, mechanism, and relevant upgrading for improving process efficiency, Biotechnology for Biofuels and Bioproducts 2022 15:1 15 (2022) 1–43. https://doi.org/10.1186/S13068-022-02203-0.

[10] A.M. Robinson, J.E. Hensley, J. Will Medlin, Bifunctional Catalysts for Upgrading of Biomass-Derived Oxygenates: A Review, ACS Catal 6 (2016) 5026–5043. https://doi.org/10.1021/acscatal.6b00923

[11] N. Agnihotri, M.K. Mondal, Process parameter variation of Melia azedarach sawdust pyrolysis for fuel properties, physicochemical characterization, and in-depth speciation analysis, Biomass Convers Biorefin (2023) 1–15. https://doi.org/10.1007/S13399-023-04305-7

[12] M.B. Figueirêdo, I. Hita, P.J. Deuss, R.H. Venderbosch, H.J. Heeres, Pyrolytic lignin: a promising biorefinery feedstock for the production of fuels and valuable chemicals, Green Chemistry 24 (2022) 4680–4702. https://doi.org/10.1039/D2GC00302C.

[13] D. Guo, S. Wu, G. Lyu, H. Guo, Effect of molecular weight on the pyrolysis characteristics of alkali lignin, Fuel 193 (2017) 45–53. https://doi.org/10.1016/J.FUEL.2016.12.042.

[14] L. Fan, Y. Zhang, S. Liu, N. Zhou, P. Chen, Y. Cheng, M. Addy, Q. Lu, M.M. Omar, Y. Liu, Y. Wang, L. Dai, E. Anderson, P. Peng, H. Lei, R. Ruan, Bio-oil from fast pyrolysis of lignin:

Effects of process and upgrading parameters, Bioresour Technol 241 (2017) 1118–1126. https://doi.org/10.1016/J.BIORTECH.2017.05.129.

[15] S. Wang, Z. Wan, Y. Han, Y. Jiao, Z. Li, P. Fu, N. Li, A. Zhang, W. Yi, A review on lignin waste valorization by catalytic pyrolysis: Catalyst, reaction system, and industrial symbiosis mode, J Environ Chem Eng 11 (2023) 109113. https://doi.org/10.1016/J.JECE.2022.109113.

[16] N. Agnihotri, M.K. Mondal, Comparison of non-catalytic and in-situ catalytic pyrolysis of Melia azedarach sawdust, J Anal Appl Pyrolysis 172 (2023) 106006. https://doi.org/10.1016/J.JAAP.2023.106006.

[17] M.W. Nolte, B.H. Shanks, A Perspective on Catalytic Strategies for Deoxygenation in Biomass Pyrolysis, Energy Technology 5 (2017) 7–18. https://doi.org/10.1002/ENTE.201600096.

[18] J. Yan, Z. Li, Y. Zhang, R. Liu, L. Zhou, P. Fu, Hydrodeoxygenation of lignin phenolic derivatives to aromatics: A review of catalyst functionalization for targeted deoxygenation and active site modification strategies, Fuel Processing Technology 250 (2023) 107914. https://doi.org/10.1016/J.FUPROC.2023.107914.

[19] P. Sun, Z. Wang, C. Li, B. Tang, C. Peng, Catalytic conversion of lignin and its derivatives to alkanes over multifunctional catalysts: A review, Fuel 361 (2024) 130726. https://doi.org/10.1016/J.FUEL.2023.130726.

[20] S. Adeyeye Nafiu, A.M. Ajeebi, H.S. Alghamdi, M.A. Aziz, M. Nasiruzzaman Shaikh, Solid-Supported Catalysts for Organic Functional Group Transformations, Asian J Org Chem 12 (2023) 163–190. https://doi.org/10.1002/AJOC.202300051.

[21] M.A. Bazhenova, L.A. Kulikov, Y.S. Bolnykh, A.L. Maksimov, E.A. Karakhanov, Palladium catalysts based on porous aromatic frameworks for vanillin hydrogenation: Tuning the activity and selectivity by introducing functional groups, Catal Commun 170 (2022) 106486. https://doi.org/10.1016/J.CATCOM.2022.106486.

[22] C. González, P. Marín, F. V. Díez, S. Ordóñez, Gas-Phase Hydrodeoxygenation of Benzaldehyde, Benzyl Alcohol, Phenyl Acetate, and Anisole over Precious Metal Catalysts, Ind Eng Chem Res 55 (2016) 2319–2327. https://doi.org/10.1021/acs.iecr.6b00036.

[23] H. Kim, J. Lee, Y. Kim, J.-M. Ha, Y.-K. Park, D.G. Vlachos, Y.-W. Suh, J. Jae, Continuous flow upgrading of lignin pyrolysis oils to drop-in bio-hydrocarbon fuels over noble metal catalysts, Chemical Engineering Journal 481 (2024) 148328. https://doi.org/10.1016/J.CEJ.2023.148328.

[24] American Society for Testing and Materials, D5373 Standard Test Methods for Determination of Carbon, Hydrogen and Nitrogen in Analysis Samples of Coal and Carbon in Analysis Samples of Coal and Coke, (2021). https://www.astm.org/d5373-21.html (accessed 03-12-2024).

[25] A.S. for T. and Materials, D3172 Standard Practice for Proximate Analysis of Coal and Coke, (2021). https://www.astm.org/d3172-13r21e01.html (accessed 03-12-2024).

[26] S.L. Soled, A. Malek, S. Miseo, J. Baumgartner, C. Kliewer, M. Afeworki, P.A. Stevens, Supported metal catalysts: Some interesting new leads in an old field, Elsevier Masson SAS, 2006. https://doi.org/10.1016/S0167-2991(06)80896-7.

[27] M. Ortega, D. Gómez, R. Manrique, G. Reyes, J.T.G.- Sánchez, V.G.B. Medrano, R. Jiménez, L.E. Arteaga-Pérez, Reductive amination of phenol over Pd-based catalysts: Elucidating the role of the support and metal nanoparticle size, React Chem Eng (2022). https://doi.org/10.1039/D2RE00259K.

[28] M.A. Vannice, Kinetics of Catalytic Reactions, Springer US, Boston, MA, 2005. https://doi.org/10.1007/b136380.

[29] A.L. Patterson, The Scherrer Formula for X-Ray Particle Size Determination, Physical Review 56 (1939) 978. https://doi.org/10.1103/PhysRev.56.978.

[30] Md. Sahadat Hossain, S. Ahmed, Easy and green synthesis of TiO2 (Anatase and Rutile): Estimation of crystallite size using Scherrer equation, Williamson-Hall plot, Monshi-Scherrer

Model, size-strain plot, Halder- Wagner Model, Results in Materials 20 (2023) 100492. https://doi.org/10.1016/J.RINMA.2023.100492.

[31] Z. Ma, Q. Sun, J. Ye, Q. Yao, C. Zhao, Study on the thermal degradation behaviors and kinetics of alkali lignin for production of phenolic-rich bio-oil using TGA-FTIR and Py-GC/MS, J Anal Appl Pyrolysis 117 (2016) 116–124. https://doi.org/10.1016/j.jaap.2015.12.007.

[32] Z. Zhang, Z. Li, H. Zhang, C. Ma, Z. Zhang, Y. Xie, S. Liu, Q. Wang, C.U. Pittman, Selective catalytic conversion of Kraft lignin into monoaromatic hydrocarbons over niobium oxide catalysts, Fuel Processing Technology 235 (2022) 107382. https://doi.org/10.1016/j.fuproc.2022.107382.

[33] J.A. Santana Junior, W.S. Carvalho, C.H. Ataíde, Catalytic effect of ZSM-5 zeolite and HY-340 niobic acid on the pyrolysis of industrial kraft lignins, (2017). https://doi.org/10.1016/j.indcrop.2017.10.023.

[34] X. Du, S. Wu, Effect of lignin modification on the selectivity of pyrolysis products from softwood kraft lignin, J Anal Appl Pyrolysis 179 (2024) 106517. https://doi.org/10.1016/J.JAAP.2024.106517.

[35] H.W. Ryu, H.W. Lee, J. Jae, Y.K. Park, Catalytic pyrolysis of lignin for the production of aromatic hydrocarbons: Effect of magnesium oxide catalyst, Energy 179 (2019) 669–675. https://doi.org/10.1016/J.ENERGY.2019.05.015.

[36] Z. Luo, K. Lu, Y. Yang, S. Li, G. Li, Catalytic fast pyrolysis of lignin to produce aromatic hydrocarbons: optimal conditions and reaction mechanism, (2019). https://doi.org/10.1039/c9ra02538c.

[37] S. Vichaphund, P. Wimuktiwan, C. Soongprasit, V. Sricharoenchaikul, D. Atong, Aromatic and aliphatic production of catalytic pyrolysis of lignin using ZSM-5/Al-SBA-15 catalyst derived from high-calcium fly ash, Energy Reports 7 (2021) 232–247. https://doi.org/10.1016/J.EGYR.2021.07.127.

[38] B.S. Azócar, P.O. Vargas, C. Campos, F. Medina, L.E. Arteaga-Pérez, Dataset from analytical pyrolysis assays for converting waste tires into valuable chemicals in the presence of noble-metal catalysts, Data Brief 40 (2022) 107745. https://doi.org/10.1016/J.DIB.2021.107745.

[39] M. Tripathi, J.N. Sahu, P. Ganesan, Effect of process parameters on production of biochar from biomass waste through pyrolysis: A review, Renewable and Sustainable Energy Reviews 55 (2016) 467–481. https://doi.org/10.1016/J.RSER.2015.10.122.

[40] T.R. Brazil, R.N. Costa, M. Massi, M.C. Rezende, Structural, morphological, and thermal characterization of kraft lignin and its charcoals obtained at different heating rates, Mater Res Express 5 (2018) 045502. https://doi.org/10.1088/2053-1591/AAB7C2.

[41] X. Dou, X. Jiang, W. Li, C. Zhu, Q. Liu, Q. Lu, X. Zheng, H. min Chang, H. Jameel, Highly efficient conversion of Kraft lignin into liquid fuels with a Co-Zn-beta zeolite catalyst, Appl Catal B 268 (2020) 118429. https://doi.org/10.1016/J.APCATB.2019.118429.

[42] A. Tagami, C. Gioia, M. Lauberts, T. Budnyak, R. Moriana, M.E. Lindström, O. Sevastyanova, Solvent fractionation of softwood and hardwood kraft lignins for more efficient uses: Compositional, structural, thermal, antioxidant and adsorption properties, Ind Crops Prod 129 (2019) 123–134. https://doi.org/10.1016/J.INDCROP.2018.11.067.

[43] I.F. Demuner, F.J.B. Gomes, M.R. Coura, J.S. Gomes, A.J. Demuner, A.M.M.L. Carvalho, C.M. Silva, Determination of chemical modification of eucalypt kraft lignin after thermal treatment by Py-GC–MS, J Anal Appl Pyrolysis 156 (2021) 105158. https://doi.org/10.1016/J.JAAP.2021.105158.

[44] M.J. Suota, T.A. da Silva, S.F. Zawadzki, G.L. Sassaki, F.A. Hansel, M. Paleologou, L.P. Ramos, Chemical and structural characterization of hardwood and softwood LignoForce™ lignins, Ind Crops Prod 173 (2021) 114138. https://doi.org/10.1016/J.INDCROP.2021.114138.

[45] W. Zhou, H. Zhang, F. Chen, Modified lignin: Preparation and use in reversible gel via Diels-Alder reaction, Int J Biol Macromol 107 (2018) 790–795. https://doi.org/10.1016/J.IJBIOMAC.2017.09.052.

[46] Z. Dong, H. Yang, P. Chen, Z. Liu, Y. Chen, L. Wang, X. Wang, H. Chen, Lignin Characterization and Catalytic Pyrolysis for Phenol-Rich Oil with TiO2-Based Catalysts, Energy and Fuels 33 (2019) 9934–9941. https://doi.org/10.1021/acs.energyfuels.9b02341

[47] C.G. Boeriu, D. Bravo, R.J.A. Gosselink, J.E.G. Van Dam, Characterisation of structure-dependent functional properties of lignin with infrared spectroscopy, Ind Crops Prod 20 (2004) 205–218. https://doi.org/10.1016/J.INDCROP.2004.04.022.

[48] K. Soongprasit, V. Sricharoenchaikul, D. Atong, Phenol-derived products from fast pyrolysis of organosolv lignin, Energy Reports 6 (2020) 151–167. https://doi.org/10.1016/J.EGYR.2020.08.040.

[49] N. Agnihotri, M.K. Mondal, Thermal analysis, kinetic behavior, reaction modeling, and comprehensive pyrolysis index of soybean stalk pyrolysis, Biomass Convers Biorefin 14 (2024) 14977–14992. https://doi.org/10.1007/s13399-023-03807-8.

[50] M. Zhang, F.L.P. Resende, A. Moutsoglou, D.E. Raynie, Pyrolysis of lignin extracted from prairie cordgrass, aspen, and Kraft lignin by Py-GC/MS and TGA/FTIR, J Anal Appl Pyrolysis 98 (2012) 65–71. https://doi.org/10.1016/J.JAAP.2012.05.009.

[51] M. Thommes, K. Kaneko, A. V. Neimark, J.P. Olivier, F. Rodriguez-Reinoso, J. Rouquerol, K.S.W. Sing, Physisorption of gases, with special reference to the evaluation of surface area and pore size distribution (IUPAC Technical Report), Pure and Applied Chemistry 87 (2015) 1051–1069. https://doi.org/10.1515/pac-2014-1117.

[52] S. Ghysels, L.E. Arteaga-Pérez, A.E. Léon, T. Menares, S. Backx, S. Mangelinckx, F. Ronsse, High Phenol Yields from Catalytic Hydropyrolysis of Lignin and Phenolic-Rich Raffinate, ACS Sustain Chem Eng 11 (2023) 13765–13777. https://doi.org/10.1021/acssuschemeng.3c03990.

[53] L. Li, W. Han, J. Zhang, G. Lu, Z. Tang, Controlled pore size of 3D mesoporous Cu-Ce based catalysts and influence of surface textures on the CO catalytic oxidation, Microporous and Mesoporous Materials 231 (2016) 9–20. https://doi.org/10.1016/J.MICROMESO.2016.05.018.

[54] G. Leofanti, M. Padovan, G. Tozzola, B. Venturelli, Surface area and pore texture of catalysts, Catal Today 41 (1998) 207–219. https://doi.org/10.1016/S0920-5861(98)00050-9.

[55] L. Di, J. Zhang, M. Craven, Y. Wang, H. Wang, X. Zhang, X. Tu, Dehydrogenation of formic acid over Pd/C catalysts: insight into the cold plasma treatment, Catal Sci Technol 10 (2020) 6129–6138. https://doi.org/10.1039/D0CY00055H.

[56] C.M. Mendez, H. Olivero, D.E. Damiani, M.A. Volpe, On the role of Pd β-hydride in the reduction of nitrate over Pd based catalyst, Appl Catal B 84 (2008) 156–161. https://doi.org/10.1016/J.APCATB.2008.03.019.

[57] A.I. Alharthi, I. Ud Din, M.A. Alotaibi, A. Bagabas, A. Naeem, A. Alkhalifa, Low temperature green methanol synthesis by CO2 hydrogenation over Pd/SiO2 catalysts in slurry reactor, Inorg Chem Commun 142 (2022) 109688. https://doi.org/10.1016/J.INOCHE.2022.109688.

[58] M. Ortega, D. Gómez, R. Manrique, G. Reyes, J.T. García-Sánchez, V.G. Baldovino Medrano, R. Jiménez, L.E. Arteaga-Pérez, Reductive amination of phenol over Pd-based catalysts: elucidating the role of the support and metal nanoparticle size, React Chem Eng 8 (2022) 47–63. https://doi.org/10.1039/D2RE00259K.

[59] C.A. Teles, P.M. de Souza, R.C. Rabelo-Neto, M.B. Griffin, C. Mukarakate, K.A. Orton, D.E. Resasco, F.B. Noronha, Catalytic upgrading of biomass pyrolysis vapors and model compounds using niobia supported Pd catalyst, Appl Catal B 238 (2018) 38–50. https://doi.org/10.1016/J.APCATB.2018.06.073.

[60] A. Corma, H. García, Lewis Acids: From Conventional Homogeneous to Green Homogeneous and Heterogeneous Catalysis, Chem Rev 103 (2003) 4307–4365. https://doi.org/10.1021/CR030680Z.

[61] P. Castaño, B. Pawelec, J.L.G. Fierro, J.M. Arandes, J. Bilbao, Enhancement of pyrolysis gasoline hydrogenation over Pd-promoted Ni/SiO2–Al2O3 catalysts, Fuel 86 (2007) 2262–2274. https://doi.org/10.1016/J.FUEL.2007.01.020.

[62] Z. Weng, F. Zaera, Sub-Monolayer Control of Mixed-Oxide Support Composition in Catalysts via Atomic Layer Deposition: Selective Hydrogenation of Cinnamaldehyde Promoted by (SiO2-ALD)-Pt/Al2O3, ACS Catal 8 (2018) 8513–8524. https://doi.org/10.1021/acssuschemeng.3c03990.

[63] C.A. Emeis, Determination of Integrated Molar Extinction Coefficients for Infrared Absorption Bands of Pyridine Adsorbed on Solid Acid Catalysts, J Catal 141 (1993) 347–354. https://doi.org/10.1006/JCAT.1993.1145.

[64] Q. Wu, G. Zhang, M. Gao, S. Cao, L. Li, S. Liu, C. Xie, L. Huang, S. Yu, A.J. Ragauskas, Clean production of 5-hydroxymethylfurfural from cellulose using a hydrothermal/biomass-based carbon catalyst, J Clean Prod 213 (2019) 1096–1102. https://doi.org/10.1016/J.JCLEPRO.2018.12.276.

[65] J. Chen, Y. Zhang, Z. Zhang, D. Hou, F. Bai, Y. Han, C. Zhang, Y. Zhang, J. Hu, Metal–support interactions for heterogeneous catalysis: mechanisms, characterization techniques and applications, J Mater Chem A Mater 11 (2023) 8540–8572. https://doi.org/10.1039/D2TA10036C.

[66] C. Amorim, M.A. Keane, Palladium supported on structured and nonstructured carbon: A consideration of Pd particle size and the nature of reactive hydrogen, J Colloid Interface Sci 322 (2008) 196–208. https://doi.org/10.1016/J.JCIS.2008.02.021.

[67] E. Leng, Y. Guo, J. Chen, S. Liu, J. E, Y. Xue, A comprehensive review on lignin pyrolysis: Mechanism, modeling and the effects of inherent metals in biomass, Fuel 309 (2022) 122102. https://doi.org/https://doi.org/10.1016/j.fuel.2021.122102.

[68] Q. Meng, J. Yan, R. Wu, H. Liu, Y. Sun, N.N. Wu, J. Xiang, L. Zheng, J. Zhang, B. Han, Sustainable production of benzene from lignin, Nature Communications 2021 12:1 12 (2021) 1–12. https://doi.org/10.1038/s41467-021-24780-8.

[69] M. Lu, J. Zhu, M. Li, Y. Shan, M. He, C. Song, TiO2-Modified Pd/SiO2 for Catalytic Hydrodeoxygenation of Guaiacol, Energy and Fuels 30 (2016) 6671–6676. https://doi.org/10.1021/ACS.ENERGYFUELS.6B00787.

[70] J. Sun, A.M. Karim, H. Zhang, L. Kovarik, X.S. Li, A.J. Hensley, J.S. McEwen, Y. Wang, Carbon-supported bimetallic Pd–Fe catalysts for vapor-phase hydrodeoxygenation of guaiacol, J Catal 306 (2013) 47–57. https://doi.org/10.1016/J.JCAT.2013.05.020.

[71] A. Majhi, Y.K. Sharma, R. Bal, B. Behera, J. Kumar, Upgrading of bio-oils over PdO/Al2O3 catalyst and fractionation, Fuel 107 (2013) 131–137. https://doi.org/10.1016/J.FUEL.2013.01.025.

[72] Z. Zhang, Z. Li, H. Zhang, C. Ma, Z. Zhang, Y. Xie, S. Liu, Q. Wang, C.U. Pittman, Selective catalytic conversion of Kraft lignin into monoaromatic hydrocarbons over niobium oxide catalysts, Fuel Processing Technology 235 (2022) 107382. https://doi.org/10.1016/j.fuproc.2022.107382.

[73] D. Mourant, Z. Wang, M. He, X.S. Wang, M. Garcia-Perez, K. Ling, C.-Z. Li, Mallee wood fast pyrolysis: Effects of alkali and alkaline earth metallic species on the yield and composition of bio-oil, Fuel 90 (2011) 2915–2922. https://doi.org/10.1016/J.FUEL.2011.04.033.

[74] H. Yang, X. Zhu, H.W. Amini, B. Fachri, M. Ahmadi, G.H. ten Brink, P.J. Deuss, H.J. Heeres, Efficient Cu-based catalysts for the selective demethoxylation of guaiacols, Appl Catal A Gen 654 (2023) 119062. https://doi.org/https://doi.org/10.1016/j.apcata.2023.119062.

Supplementary material

Thermo-catalytic depolymerization of lignin over Pd-based catalysts: Role of catalyst support on monoaromatics selectivity

José R. Colina[1,2], Maray Ortega[1], Jose Norambuena-Contreras[3], Stef Ghysels[4], Frederik Ronsse[4], Luis E. Arteaga-Pérez[5*]

[1]Laboratory of Thermal and Catalytic Processes (LPTC), Wood Engineering Department, University of Bío-Bío, Concepción, 4030000, Chile.

[2]Facultad de Medicina y Ciencia, Universidad San Sebastián, Lientur 1457, Concepción 4080871, Chile

[3]Materials and Manufacturing Research Institute, Department of Civil Engineering, Faculty of Science and Engineering, Swansea University, Bay Campus, SA1 8EN, UK.

[4]Department of Green Chemistry and Technology, Ghent University, Coupure Links 653, Ghent 9000, Belgium

[5]Department of Chemical Engineering, Faculty of Engineering, Universidad de Concepcion, Chile

*Corresponding author: luiseap@gmail.com

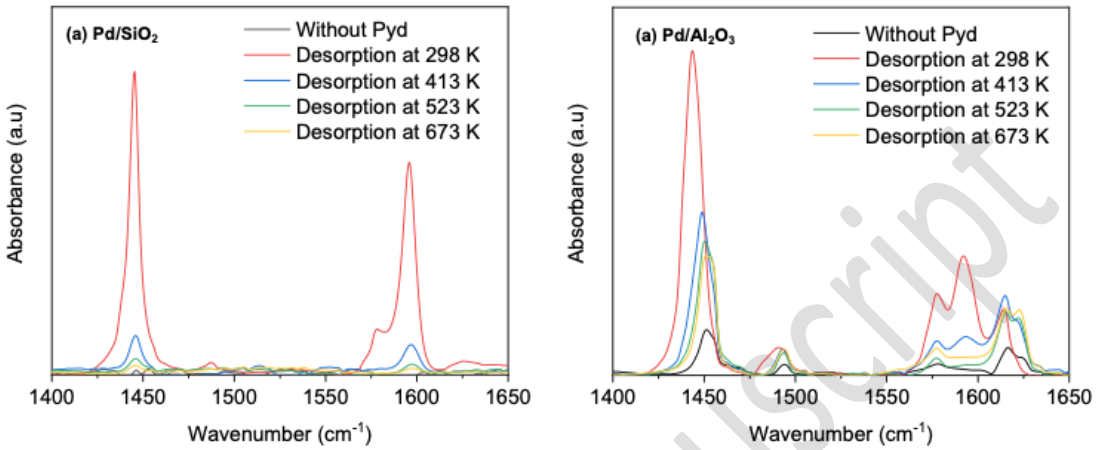

Fig. S1. FTIR spectra of pyridine desorbed at 298, 413, 523, and 673 K for (a) Pd/SiO_2 and (b) Pd/Al_2O_3 supports. Analysis was performed after catalyst reduction.

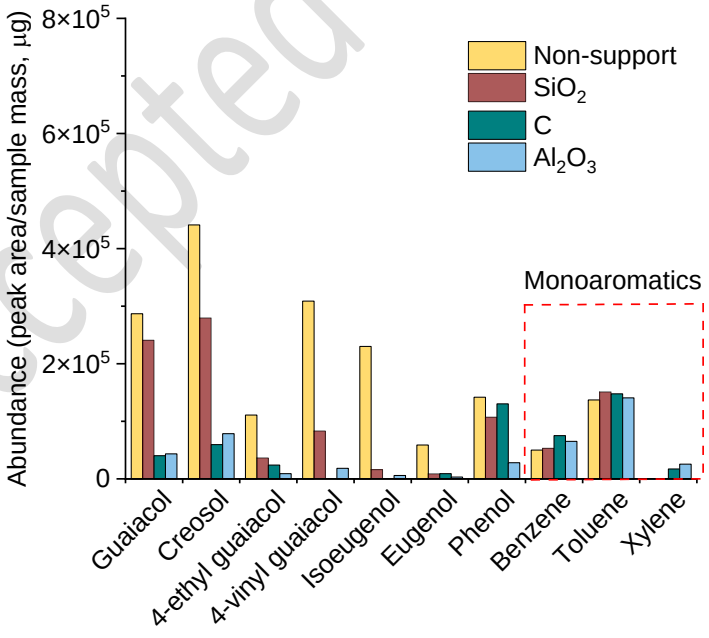

Fig. S2. Relative quantities of majority products obtained from lignin fast pyrolysis using pristine SiO_2, Al_2O_3 and activated carbon as catalyst.